AD-A126 858 CHANGES IN RESIDUAL STRESS DOMAIN SIZE AND MICROSTRAIN 1/1
DURING FATIGUE OF 1.. (U) NORTHWESTERN UNIV EVANSTON IL
DEPT OF MATERIALS SCIENCE H K KUO ET AL. 01 MAR 83
UNCLASSIFIED TR-9 N00014-80-C-0116 F/G 11/6 NL

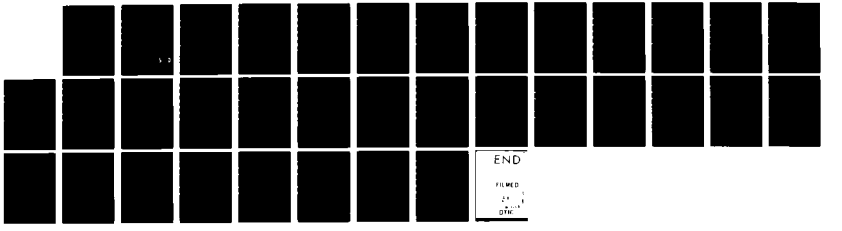

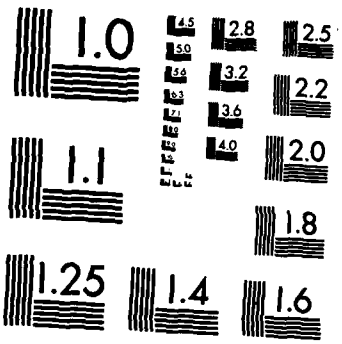

(1)

NORTHWESTERN UNIVERSITY

DEPARTMENT OF MATERIALS SCIENCE

Technical Report No. 9
March 1, 1983

Office of Naval Research
Contract N00014-80-C-0116

CHANGES IN RESIDUAL STRESS, DOMAIN SIZE AND MICROSTRAIN DURING FATIGUE OF 1008 STEEL

BY

H. K. Kuo and J. B. Cohen

EVANSTON, ILLINOIS

Changes in Residual Stress, Domain Size and Microstrain During Fatigue of 1008 Steel

by

H. K. Kuo
Institute of Materials Science and Engineering
National Sun Yat-Sen University
Kaohsiung, Taiwan, Republic of China

and

J. B. Cohen
Materials Science and Engineering
Technological Institute, Northwestern University
Evanston, Illinois 60201 USA

ABSTRACT

Changes in the positions and shapes of x-ray diffraction peaks have been examined after low-cycle and high-cycle strain-controlled fatigue of normalized and cold-worked 1008 steel. Measurements were made at and below the surface. Domain (mosaic) size is sometimes the major contributor to peak breadth, but sometimes it is controlled by microstrain, or by both quantities. Microstrains are larger after low-cycle fatigue than after high-cycle fatigue. The surface residual stress is altered by fatigue, and the pattern of change with cycling is similar for low or high strains, and for initally normalized or cold-worked specimens. Near failure in low-cycle fatigue of a cold-worked specimen, the domain size and microstrain approach those for a (cycled) annealed specimen. Dislocation densities are the order of 10^{13}-10^{14} per m^2. Cycling in the initially normalized condition increases both the dislocation density and dislocation arrangements with low long-range strain. However, with cold-worked 100^{p} steel, the density decreases and, near failure, the dislocation array is nearly random. In all cases, the peak breadth passes through a minimum vs. depth below the surface. In low-cycle fatigue of the normalized condition, the damage is less in the interior than at the surface, but after high-cycle fatigue, (and after high or low-cycle fatigue of cold-worked samples) the damage is greater in the interior of a specimen. The dislocation arrangement oscillates with depth, below the surface, at least for the first few hundred microns.

INTRODUCTION

In early studies of the effects of fatigue on the x-ray diffraction pattern, Taira and co-workers (1-3) found that the breadth of a diffraction peak (from the ferrite) in the surface of an annealed low-carbon steel changed in three distinct stages: 1) a marked increase early in life, 2) an extended number of cycles with only a slight increase, 3) another marked increase coinciding with crack initiation. Measurements of the residual stresses in the same investigations indicated that compressive stresses developed initially, then decreased to a near zero at the onset of cracking. These tests were performed in bending. However, in tension-tension fatigue the compressive stresses decreased only slightly, although the changes in breadth were similar (4). Surprisingly, compressive stresses produced by shot peening rapidly changed to tensile values. Taira and Hayashi (5) reported a fourth stage of increasing peak breadth near a crack, apparently due to fatigue crack growth and its attendant plastic flow (and this was confirmed in Ref. 4). These authors (5) and Hayashi et al (6) pursued these studies further by examining the changes in breadth and stress vs depth below the surface, and as well, hardness. They reported that up to 30-100 μm below the surface, changes in breadth and stress continued throughout fatigue life, whereas changes in hardness occurred only in the initial cycles. At greater depths, breadth increased initially, but stresses changed very little.

Pangborn et al (7) determined the excess dislocation density by measuring rocking curves of individual grains in a coarse-grained Al alloy and found a similar three-stage effect. However, if Mo rather than Cu radiation was employed (to sample greater depths) the changes were linear throughout the cycling and failure occurred at some fixed critical excess dislocation density regardless of strain, as was first suggested by Kramer (8). (While these

authors proposed employing this phenomenon in the field for nondestructive evaluation of remaining fatigue life, the effects are not the same in all grains, and it is unlikely that such an evaluation is practical with a real part.)

Only a few attempts have been made to understand the nature of the x-ray peak broadening in fatigue. With a normalized 0.16% C steel, Taira et al (9) used Hall's method (10) to separate the effects due to domain (mosaic) size and average microstrain. While this procedure is quite approximate, they reported that microstrains initially increased with cycling, then remained essentially constant for the remainder of fatigue life (except for a small decrease just prior to fracture, which the authors attributed to polygonization). The domain size decreased continuously during fatigue. In a second paper Taira and co-workers (11) used the more complete Fourier analysis of peak shapes (12), and compared uniaxial tension and (low-cycle) fatigue. In tension, domain size decreased rapidly during the initial plastic strain, and subsequently did not change appreciably. On the other hand, rms microstrains increased continuously with strain. In contrast to this behavior, during (strain controlled) fatigue, with $R = -1$, the changes in both parameters were complete early in the fatigue life, and did not change significantly until close to failure. Decreasing the total strain from 2.56 to 2.0 pct caused a marked decrease in microstrain. The x-ray parameters of domain size and microbtrain oscillated with cycling. The domain size was larger (by almost a factor or two) in fatigue than in tension.

In this investigation we extend such studies to include high-cycle fatigue, and as well, how the effects vary with depth below the surface. While it is well known that cold-worked materials often soften during fatigue, it is not clear how similar is the microstructure near failure in this case, to that after fatigue in the initially annealed condition. This point was also

examined. Inferences are drawn about the dislocation arrangements from the results.

EXPERIMENTAL PROCEDURES

Materials and Preparation

Starting with 0.032 m. diameter rods of AISI 1008 steel, two sets of specimens were prepared. The first set were machined to the dimensions shown in Fig. 1, and normalized by annealing for one hour in Argon gas at 1193°K, followed by an air cool. Oxidized and decarburized layers were removed by polishing through (wet) 600 grit SiC paper, to remove 100 μm from each face. This was followed by a chemical polish in an H_2O_2-HF solution kept at 283°K, to remove an additional 150 μm. The grain size was 23 μm. A set of cold-worked specimen were obtained from the rods by machining into blocks 0.05 x 0.025 x .012m, and rolling to a 50 pct reduction in thickness, 2.5×10^{-5} m per pass. Two specimens (as in Fig. 1) were cut from each such slab, and were then surface ground to obtain parallel surfaces, with a down feed of 2.5×10^{-5} m per pass, finishing with a down feed of 1.2×10^{-5} m per pass. These specimens were polished following the same procedures used for the normalized material.

Fatigue was carried out on a 100 KN capacity closed loop servo-controlled electrohydraulic machine, (manufactured by MTS). Specimen alignment was achieved by melting a Wood's metal bath containing one grip, prior to applying the full load. The tests were performed in strain control, with a fully-reversed triangular strain wave, with a total strain amplitude of 0.7 pct and with a strain rate of 2×10^{-3} sec^{-1} for low-cycle fatigue. These values were 0.15 pct and 1.5×10^{-3} sec^{-1} for high-cycle fatigue. Specimens were removed at various stages to examine the diffraction pattern, by slowly reducing the strain amplitude in stages (to zero), while maintaining the strain

rate. The specimens and the x-ray sample holder were marked to ensure that the same area was always examined. Changes in the x-ray pattern with depth below the surface were studied after various numbers of cycles by chemically polishing an area in the gage length on one face.

The x-ray diffraction patterns were obtained with the aid of an automated Huber θ-2θ goniometer and a scintillation detector. The CoK_α radiation from a Co x-ray tube used in line focus at 4° take off angle, and operated at 40KV, 15 ma. The distance from the target to the sample, and from the sample to the receiving slit was 0.173 m. For recording 110 and 220 peak profiles, a 1° divergent slit was employed, with a scatter slit, soller baffle and a 0.0016° receiving slit in front of the detector. The profiles were recorded by step scanning in intervals of 0.005° - 0,01° 2θ in the peak, and 0.05° 2θ in the background, counting for 10-50 seconds after each step. Typical counts were, for the 110 peak: 50 in the background, 2000 - 4000 in the peak, and for the 220: 350 in the background, 1000 - 1500 in the peak. Fourier analysis (12) of these peak shapes was employed to obtain information from the cosine coefficients on both the average mosaic size (D) and rms. microstrain $\langle \varepsilon^2 \rangle^{1/2}$. The reported microstrains are average values over all columns 400Å long under the x-ray beam. To correct for instrumental broadening, the method of Stokes was employed (13), with a specimen prepared by annealing in Argon at 920°C for 3 hrs., and furnace cooling overnight. (This standard was polished as described above for the normalized condition.) Prior to the Fourier analysis, a computer code was utilized to separate the K_α component of each doublet peak (14). The Fourier analysis was carried out about each peak's center of gravity, to minimize the sine coefficients, and the cosine coefficients were normalized following Ref. 15.

Residual stresses were measured in the direction of the load, with the 220 peak ($2\theta \cong 124^{o}$), and with a 0.033^{o} receiving slit. These measurements were automated (16). To locate a peak's position, a five-point parabolic fit to the top 15 pct of a peak (after background subtraction) was employed. Six sample tilts (ψ) between 0 and 45^{o} were used to ensure linearity of interplanar spacing vs $\sin^2 \psi$, as required for simple surface stress measurements. The specimen was aligned (via a software routine) to within 1.2×10^{-5} m of the center of the diffractometer, by using the lattice parameter obtained from low and high-angle peaks to calculate sample displacement. The x-ray elastic constants were calculated from the single crystal constants of Fe (17), assuming an average of constant stress and constant strain. Measurements were taken to an operator-specified precision in terms of stress. The geometric error was 10 MPa and the statistical error was ± 20 MPa.

In these x-ray studies, the X-ray beam sampled an area of 4×10^{-3} by 2×10^{-3} mm, and the penetration depth was 14 μm for the 110 peak, 28μm for the 220 peak. No correction was made to the stress mesurements for this depth, as the correction was 10 pct or less. In the studies vs. depth, below the surface, corrections were made for layer removal (18).

RESULTS

Visual Observations

Deformation markings, similar to Luder's bands and covering most of the reduced section, formed on all specimens, except for those which were cold-worked and deformed in high-cycle fatigue. These markings were most pronounced for the normalized condition subjected to low-cycle fatigue.

Normalized Condition-Changes Near the Surface

The results for low-cycle fatigue ($\Delta\epsilon/_2 = 0.7$ pct, life$\cong$ 1600 cycles),

are presented in Fig. 2. The breadth of the 220 peak exhibits three stages, as reported in refs. 1-3 and 7. It is smallest before fatigue, increases rapidly during the first 100 cycles, and is then nearly constant until 900 cycles, when it increases again and continues to do so until failure. The domain size (D) decreases continuously with cycling until about 900 cycles, after which it increases until failure (which confirms results in ref. 1). The rms microstrains remain nearly constant until 900 cycles and then increase, again similar to results in (1) for $\Delta\varepsilon/2$ = 1.0 pct. Therefore, peak breadth is initially controlled by domain size, but subsequently follows changes in the microstrains. The pattern of changes in residual stress with cycling is somewhat similar to that for domain size, and these stresses reach a maximum compressive value of -400 MPa, increase to -300 MPa at 900 cycles, then remain unchanged until failure, in agreement with (15).

The data for high-cycle fatigue ($\Delta\varepsilon/2$ = 0.15 pct, life 85,000 cycles) are given in Fig. 3. In contrast to low-cycle fatigue, peak breadth initially decreases, then remains nearly constant until $\approx$ 60,000 cycles, after which it increases to failure. By comparing these trends with those for D and $<\varepsilon^2>^{1/2}$, it is clear that the changes in peak breadth are due mainly to changes in domain size throughout cycling, because the microstrains do not change appreciably in high-cycle fatigue. Again the changes in stress follow the pattern of changes in D, but in contrast to low-cycle fatigue, an increase in (compressive) stress is associated with an increase in domain size. Clearly, it is not possible to link the residual stresses to only one or the other of the microstructural parameters, (D or $<\varepsilon^2>^{1/2}$). The maximum compressive stress is approximately 10 pct less than in low-cycle fatigue, and the pattern of change in stress with cycling is quite similar to that for low-cycle fatigue. Near failure, the microstrains and average domain size are quite

different after low or high-cycle fatigue.

Cold-Worked Condition-Changes Near the Surface

The results for low-cycle fatigue ($\Delta\varepsilon/2$ = 0.7 pct, life = 1300 cycles) and for high-cycle fatigue ($\Delta\varepsilon/2$ = 0.15 pct, life = 95,000 cycles) are given in Figs. 4 and 5. For both, peak breadth is dependent on D and $\langle \varepsilon^2 \rangle^{1/2}$ throughout cycling. While the pattern of changes is quite similar for both fatigue strains, the changes in microstrain and domain size are much larger in low-cycle fatigue, whereas the stresses that develop during both kinds of fatigue are similar in magnitude.

Comparing the changes for the normalized and cold-worked condition: 1) the compressive stresses that develop are larger by nearly a factor of two for the normalized steel; 2) the pattern of stress change with cycling is the same for both initial conditions and for low-cycle and high-cycle fatigue; 3) the changes in stress follow the microstrains in the cold-worked samples, but not in the normalized condition; 4) in low-cycle fatigue, near failure, D and $\langle \varepsilon^2 \rangle^{1/2}$ are similar for both specimen conditions. In high cycle-fagigue, D is similar for both initial conditions, but the microstrains are much lower in the cold-worked steel; 5) there is evidence for saturation of microstrains in high-cycle fatigue for both conditions, whereas this occurs for both D and $\langle \varepsilon^2 \rangle^{1/2}$ in low-cycle fatigue.

Normalized Condition-Changes vs Depth

a) Low-Cycle Fatigue

Specimens were fatigued to 100, 1150 and 1600 cycles (the latter value is 95 pct of the life). Measurements were made vs depth, by removing layers with the chemical polish described in the procedures. After 1600 cycles, the specimen had a large visible crack, and the X-ray beam was placed over this.

The 220 peak breadth was larger in this vicinity than in the other specimens discussed above, indicating an increase associated with the plastic zone, in agreement with ref. 15.

The results are summarized in Figs. 6-8. In all cases, the breadth decreases with depth for the first 200-300 μm, and then increases, but never reaches the value at the surface. This result is in agreement with Pangborn et al (7), but in disagreement with Mughrabi et al (19). The changes in domain size and microstrain are quite different for the specimen close to failure, compared to the other two. For example, after 100 and 1150 cycles, both the domain size and microstrain <u>decrease</u> in the first 50 - 100 μ m, whereas these parameters <u>increase</u> with depth after 1600 cycles. Note that the microstrains at the interior of the cracked specimen are substantially greater than those after 100 or 1150 cycles. Also, after 1150 and 1600 cycles the compressive stress increases in magnitude for the first ~ 100 μm, but after only 100 cycles, these decrease over the same depth. This confirms results in ref. 3.

b) <u>High-Cycle Fatigue</u>

Two normalized specimens were fatigued to 60,000 and 78,340 cycles respectively (at $\Delta\varepsilon/2$ = 0.15 pct). For the former, the 220 peak breadth vs depth is similar to the pattern observed in low-cycle fatigue. After 78,340 cycles, the specimen contained small cracks, and the data are given in Fig. 9. In this case, the breadth also passes through a minimum at about 100 μm, but is even larger at 400 μm than at the surface, probably due to the cracks.

Comparing the depth profiles, low-vs high-cycle fatigue near failure (Figs. 8 and 9), it is clear that the patterns for stress, domain size and microstrain vs depth are alike. The changes are much greater, however, for high-cycle fatigue, and the microstrains are lower in this case.

Cold-Worked Condition-Effects vs Depth

a) Low-Cycle Fatigue

Results are summarized in Figs. 10 and 11. The minimum in breadth vs depth occurs in this case as well, but the values at 400-500 μm are larger than those at the surface, as was the case for the normalized condition near failure in high-cycle fatigue. The changes in stress vs. depth are much less than for the normalized state, and there is no evidence of a maximum in magnitude. The variation in D is much smaller, as well, although two maxima are also present in this case. The microstrains are similar to those after low-cycle fatigue in the normalized condition.

b) High-Cycle Fatigue

The results for 78,340 cycles appear in Fig. 12. Once again the peak breadth, although exhibiting a minimum 50-100 μm under the surface, is larger in the deep interior than at the surface. (After 60,000 cycles there was no minimum, just a steady increase with depth.) The domain size passes through a broad minimum, as does the microstrain. The domain size and microstrain are similar to those after high-cycle fatigue of the normalized state, but the stresses are lower.

DISCUSSION

As a summary, Fig. 13 illustrates schematically the trends observed in this investigation. The change in surface stress vs. cycling is surprisingly similar, regardless of the strain in fatigue, or the initial condition of the specimens. The pattern of peak breadth, on the other hand, varies in shape with these conditions, but even more importantly, the breadth is not an adequate description of the development of substructure. Microstrain or domain size, or both, can control the observed changes in breadth. It is interesting to note the peak sharpening that occurs after a few cycles with a normalized

steel in high-cycle fatigue. This is probably due to strain aging, and is another manifestation of this phenomenon which has already been observed during fatigue (20).

The minimum in peak breadth just below the surface reported by Pangborn et al (7) for low-cycle fatigue of annealed Aℓ alloy also occurs in steel, in high-cycle fatigue as well as low-cycle fatigue, and for the cold-worked as well as the normalized condition. However, the broadening in the interior can exceed that in the surface in some cases; high-cycle fatigue in the annealed condition, or high and low cycle fatigue in the cold-worked condition. The consistent shape of mosaic size vs depth is also striking. Furthermore, the first minimum in this size (vs depth) corresponds (approximately) to the minimum in breadth.

[We have made attempts to examine other steels for these changes, in particular 4130 (quenched and tempered for 2 hrs. at 593°C) and HY130 (quenched, or quenched and tempered for 2 hrs. at 650°C, or furnace cooled). No changes in peak breadth were observed in low-cycle fatigue, although several peaks were examined. Stresses were observed to fade.]

While we have reported our findings in terms of the parameters determined from the X-ray patterns, it is possible to interpret these in terms of the dislocation structure. If the dislocations are randomly arranged, the dislocation density (ρ) can be obtained from $1/D^2$ or $12 < \epsilon^2 > /b^2$ where b is the Burger's vector (21,22). If $\rho_D << \rho_\epsilon$, cells or subgrains exist. Comparisons of such an approach with electron microscopy are summarized in ref. 23, where it is shown that correct densities and arrangements are obtained. (This procedure is especially useful for highly deformed materials, in which

case it is difficult to measure ρ in the electron microscope.) For low-cycle fatigue of normalized steel, after 1600 cycles $\rho_D = 4 \times 10^{13}$ per m^2 and $\rho_\varepsilon = 3 \times 10^{13}$ per m^2. This indicates that at this stage, the dislocation array is close to random; cells are not well developed. This is in agreement with electron microscopic observations of pure iron and the ferrite phase in pearlitic eutectoid steel (24,25). After 1000 cycles (see Fig. 2) when the domain size is a minimum, $\rho_D = 1.2 \times 10^{14}$ m^2 and $\rho_\varepsilon = 0.1 \times 10^{14}$ $m^{2^{-1}}$. Thus, at this stage, there are many dislocation arrays (such as dipoles) which have low long-range strain fields. From such calculations the following results were obtained from the X-ray parameters:

1) In normalized specimens subjected to low-cycle or high cycle fatigue, more low-strain dislocation arrangements occur near the surface as cycling proceeds. This implies the development of highly stable dislocation walls.

2) In cold-worked specimens subjected to low-cycle or high-cycle fatigue, the dislocation density near the surface decreases by a factor of ~ 3, and becomes more random with cycling.

3) In investigations of the changes below the surface, domain size oscillates and the maxima in domain size generally correspond to near-random dislocation arrays, whereas at the minima in domain size, there are more stable arrangements with low long-range stress fields.

CONCLUSIONS

1) The breadth of x-ray peaks is not totally adequate as a measure of fatigue induced microstructure. In some situations, broadening is due primarily to domain size, in others it is dominated by microstrains, and often both are major contributors.

2) Microstrains are larger in normalized or cold worked 1008 steel after

low cycle fatigue than after high-cycle fatigue.

3) The surface residual stress is altered by fatigue and the pattern with cycling is the same for low or high strains, and for normalized or cold-worked specimens.

4) In low-cycle fatigue of a cold-worked specimen, the domain size and microstrain are altered to those found after such fatigue of an initially normalized specimen, but only the domain size is similar in high-cycle fatigue. Microstrains are much lower for cold-worked specimens than for annealed ones.

5) For a normalized steel, fatigue causes an increased density of dislocation arrays with low long-range stresses near the surface.

6) For cold worked 1008 steel, cycling decreases the disloction density and produces a more random array near the surface.

7) After cycling, in all cases studied, the peak breadth passes through a minimum vs depth. For low-cycle fatigue in the normalized condition, the damage is less in the interior than at the surface, but the reverse is true for high-cycle fatigue, or if there is severe cold work prior to (high or low-cycle) fatigue.

8) The dislocation arrangement varies cyclically with depth.

ACKNOWLEDGEMENTS

This research was supported by ONR, under grant No. N-00014-80-C-0116. The authors especially wish to thank Dr. B. McDonald (of ONR) for his encouragement, Dr. I. Kramer for informative discussions and Prof. R. J. DeAngelis (University of Kentucky) for advise in the use of his program for

doublet separation. Mr. Paul Rudnik assisted with the data processing, and Profs. Fine, J. R. Weertman and J. Weertman provided valuable comments on the manuscript. The X-ray measurements were performed in the Diffraction Facility of Northwestern University, and the fatigue was carried out in the Fatigue Laboratory there. Both facilities are supported in part by Northwestern University's Materials Research Center, under NSF grant No. DMR-MRL-76-80847.

REFERENCES

1) S. Taira, K. Honda and T. Abe, Proc. 6th Japan Congr. on Testing Materials, 1963, P. 10.

2) S. Taira, K. Honda and T. Abe, Proc. 7th Japan Congr. on Testing Materials, 1964, P. 26.

3) S. Taira and K. Hayashi, Proc. 7th Japan Congr. on Testing Materials, 1964, P. 1.

4) M. McClinton and J. B. Cohen, Materials Science and Engineering, 56 (1982) P. 259.

5) S. Taira and K. Hayashi, Proc. 7th Japan Congr. on Testing Materials, 1964, P. 38.

6) K. Hayashi, M. Yamada, N. Tohyama and N. Murase: Proc. 23rd Japan Congr. on Materials Research, 1980, P. 1.

7) R. N. Pangborn, S.Weissmann and I. R. Kramer, Met. Trans., 12A (1981) 109.

8) I. R. Kramer, Met. Trans., 5 (1974) 1735.

9) S. Taira, T.Goto and Y Nakano: Proc. 12th Japan Congress on Testing Materials, 1969, P. 8.

10) W. H. Hall, Proc. Phys. Soc. London, A62 (1949) 741.

11) S. Taira, T. Goto and Y. Nakano, Proc. 11th Japan Congr. on Testing Materials, 1968, P. 25.

12) B. E. Warren, Progr. in Metal Physics, 8 (1959) 147.

13) A. R. Stokes, Proc. Phys. Soc. London, 61 (1948) 382.

14) R. J. DeAngelis, Metallography, 6 (1973) 243.

15) R. L. Rothman and J. B. Cohen, Adv. in X-Ray Analysis, 12 (1969) 208.

16) M. R. James and J. B. Cohen, Adv. in X-Ray Analysis, 20 (1977) 291.

17) W. J. M. Tegart, McMillan Publ., 1966 (Elements of Mechanical Metallurgy, New York, New York).

18) SAE Information Report J784a, 1971, (Soc. Automotive Engineers, Inc., New York).

19) T. Ungar, H. Mughrabi and M. Wilkens, Acta Met., 30 (1982) 1861.

20) K. Pohl, P. Mayr and E. Macherauch, Int'l. Jrnl. of Fracture, in press.

21) R. E. Smallman and K. H. Westmacott, Phil. Mag., 2 (1957) 669.

22) G. K. Williamson and R. E. Smallman, Phil. Mag., 1 (1956) 34.

23) D. E. Mikkola and J. B. Cohen, J. B. Cohen and J. E. Hilliard (eds), Local Atomic Arrangements Studied by X-ray Diffraction, Gordon and Breach, New York, 1966, P. 289.

24) H. R. Pak and M. Meshii, G. Bailey (ed), 39th Ann. Proc. Electron Microscopy Society of Amer., 1981, P. 330.

25) H. Sunwoo, M. E. Fine, M. Meshii and D. H. Stone, Met. Trans., 13A (1982) 2035.

FIGURE CAPTIONS

Figure 1. Specimen dimensions (in mm).

Figure 2. a) Half-breadth of 220 peak (FWHM) and longitudinal residual stress in surface; b) Mosaic size and rms microstrain in <110> direction, vs. fatigue cycles. Normalized 1008 steel, low-cycle fatigue ($\Delta\epsilon/2$ = 0.7 pct, R = -1).

Figure 3. a) Half-breadth of 220 peak (FWHM) and longitudinal residual stress in surface; b) Mosaic size and rms microstrain in <110> direction, vs. fatigue cycles. Normalized 1008 steel, high cycle fatigue ($\Delta\epsilon/2$ = 0.15 pct, R = -1).

Figure 4. a) Half-breadth of 220 peak (FWHM) and longitudinal residual stress in surface; b) Mosaic size and rms microstrain in <110> direction, vs. fatigue cycles. Cold-worked 1008 steel, low-cycle fatigue ($\Delta\epsilon/2$ = 0.7 pct, R = -1).

Figure 5. a) Half-breadth of 220 peak (FWHM) and longitudinal residual stress in surface; b) Mosaic size and rms microstrain in <110> direction, vs. fatigue cycles. Cold-worked 1008 steel, high-cycle fatigue ($\Delta\epsilon/2$ = 0.15 pct, R = -1).

Figure 6. 12 Half breadth of 220 peak (FWHM) and longitudinal residual stress; b) Mosaic size and rms microstrain in <110> direction, vs depth. Normalized 1008 steel, low-cycle fatigue, 100 cycles ($\Delta\epsilon/2$ = 0.7 pct, R = -1).

Figure 7. a) Half breadth of 220 peak (FWHM) and longitudinal residual stress; b) Mosaic size and rms microstrain in <110> direction, vs

depth. Normalized 1008 steel, low-cycle fatigue, 1150 cycles ($\Delta\epsilon/2$ = 0.7 pct, R = -1).

Figure 8. a) Half breadth of 220 peak (FWHM) and longitudinal residual stress; b) Mosaic size and rms microstrain in <110> direction, vs depth. Normalized 1008 steel, low-cycle fatigue, 1600 cycles (~ 95 pct of life) $\Delta\epsilon/$ = 0.7 pct, R = -1.

Figure 9. a) Half breadth of 220 peak (FWHM) and longitudinal residual stress; b) Mosaic size and rms microstrain in <110> direction, vs depth. Normalized 1008 steel, high-cycle fatigue, 78,340 cycles ($\Delta\epsilon/2$ = 0.15 pct, R = -1).

Figure 10. a) Half breadth of 220 peak (FWHM) and longitudinal residual stress; b) Mosaic size and rms microstrain in <110> direction, vs depth. Cold-worked 1008 steel, low-cycle fatigue, 100 cycles ($\Delta\epsilon/2$ = 0.7 pct, R = -1).

Figure 11. a) Half breadth of 220 peak (FWHM) and logitudinal residual stress; b) Mosaic size and rms microstrain in <110> direction, vs depth. Cold-worked 1008 steel, low-cycle fatigue, 800 cycles ($\Delta\epsilon/2$ = 0.7 pct, R = -1).

Figure 12. a) Half breadth of 220 peak (FWHM) and longitudinal residual stress; b) Mosaic size and rms microstrain in <110> direction, vs depth. Cold-worked 1008 steel, high-cycle fatigue, 90,000 cycles ($\Delta\epsilon/2$ = 0.15 pct, R = -1).

Figure 13. Schematics of the changes observed.

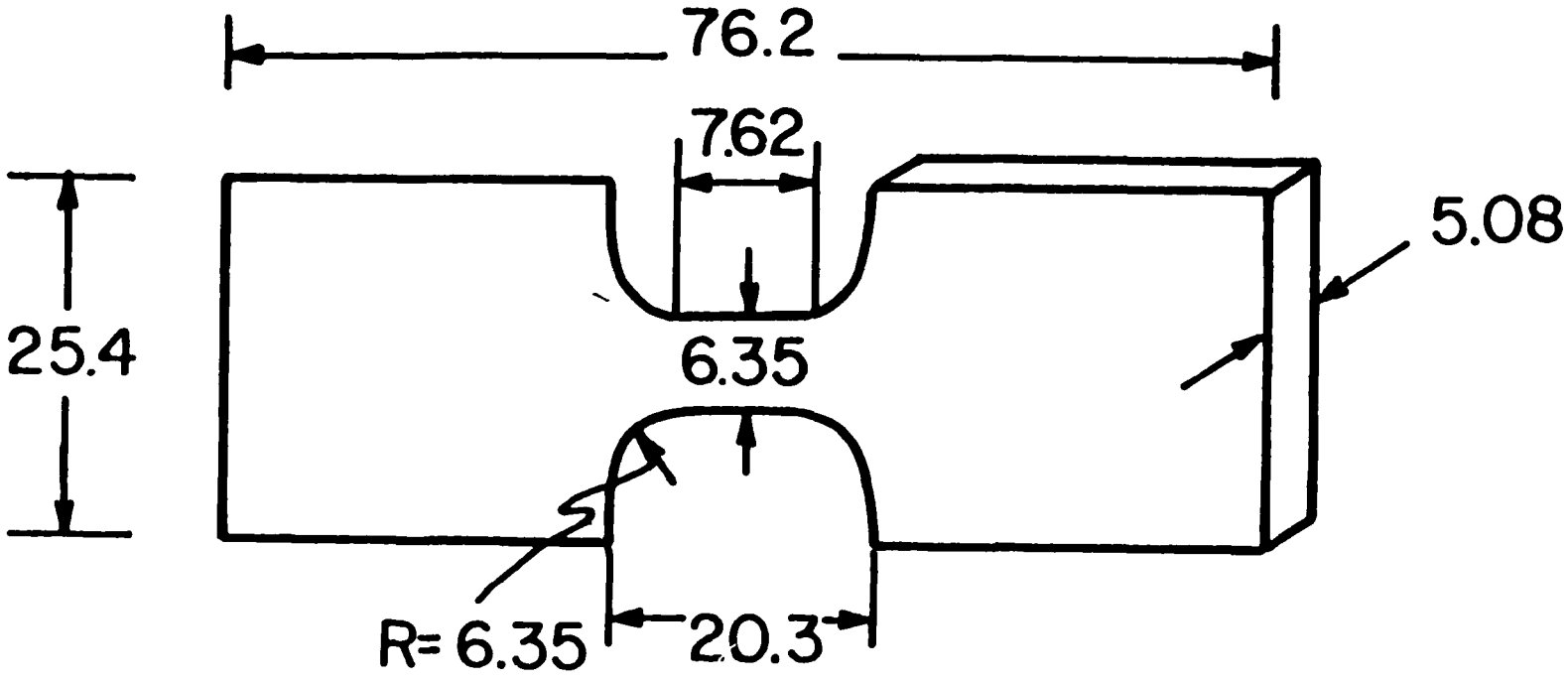

FIGURE 1

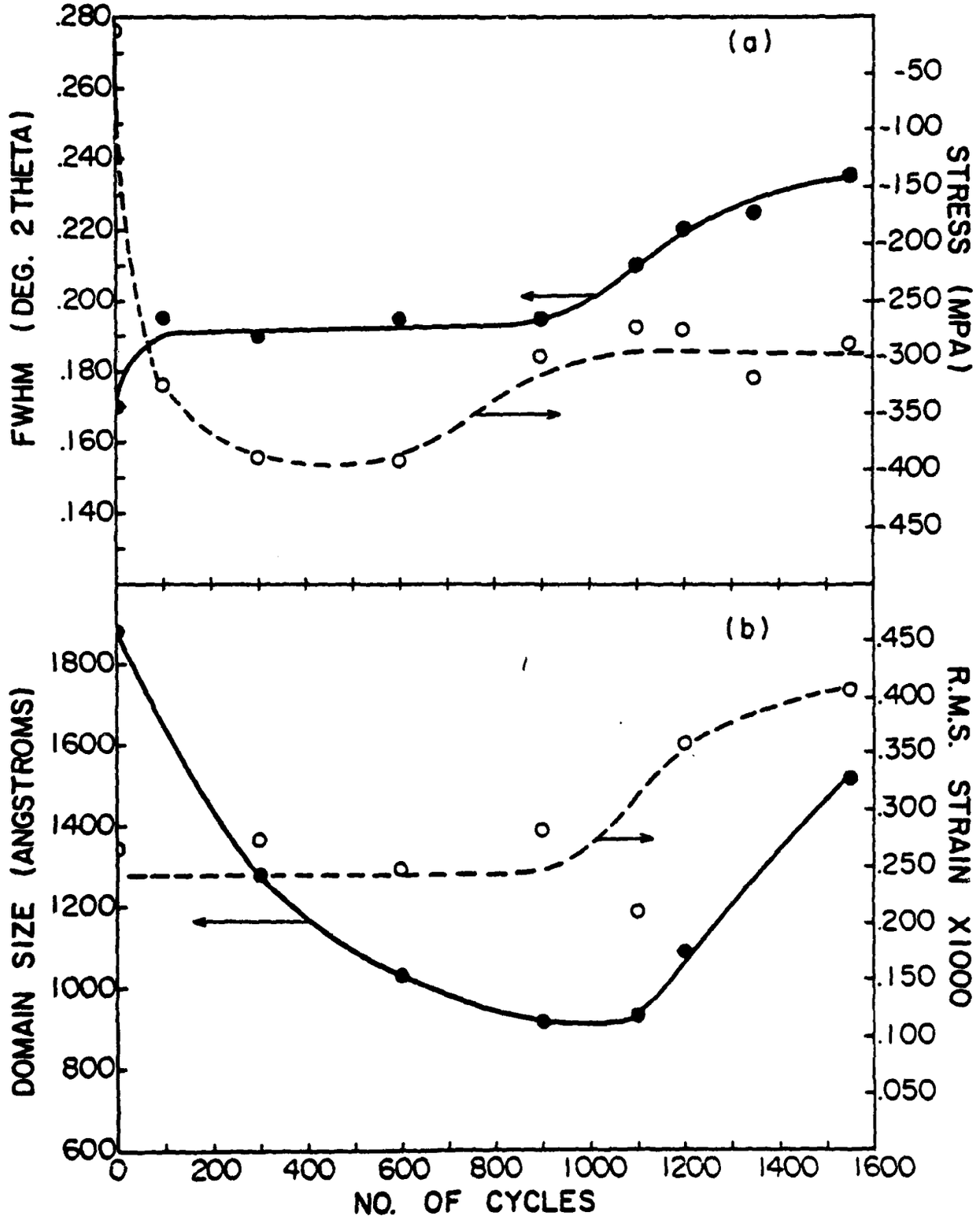

FIGURE 2

H. K. Kuo and J. B. Cohen

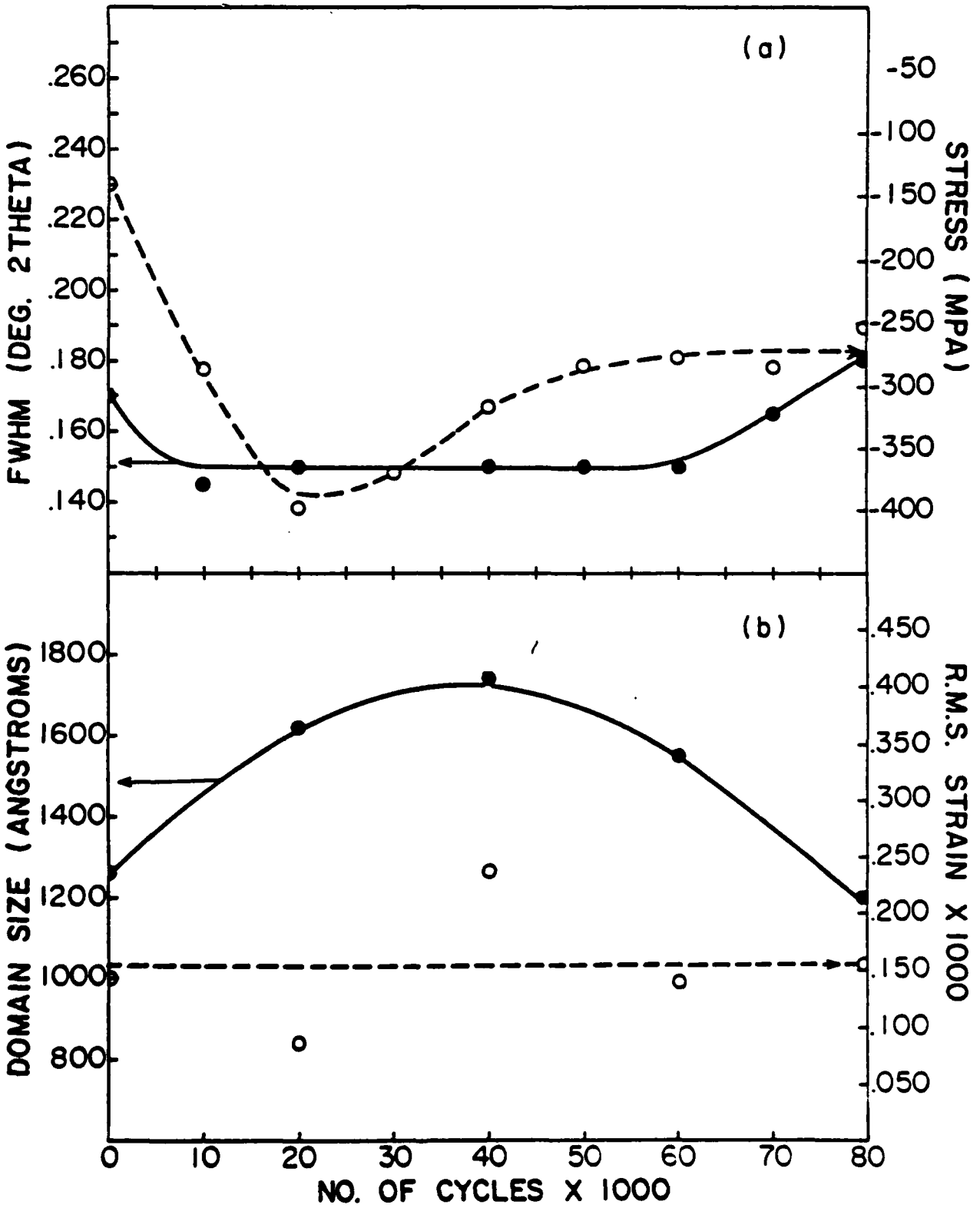

FIGURE 3

H. K. Kuo and J. B. Cohen

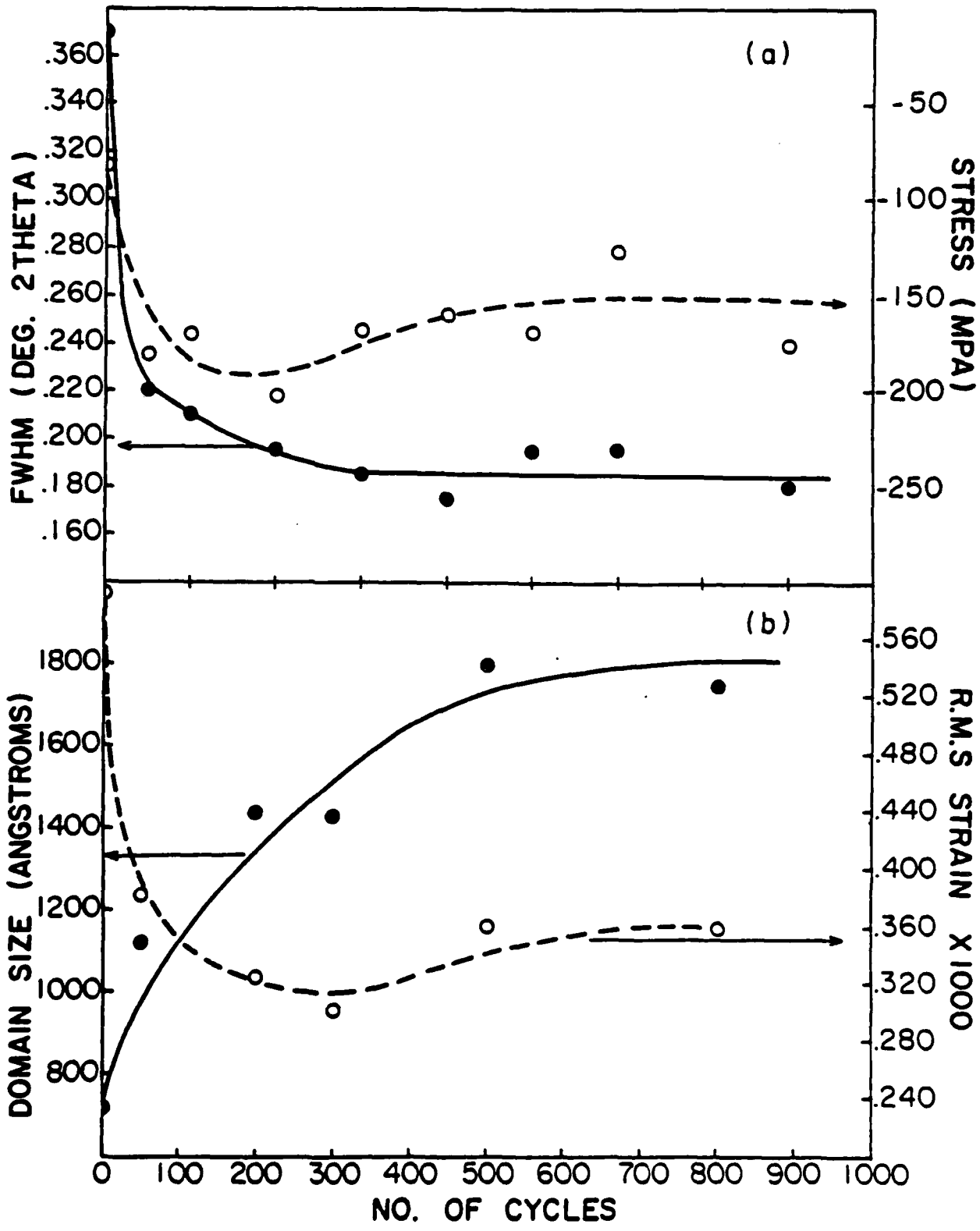

FIGURE 4

H. K. Kuo and J. B. Cohen

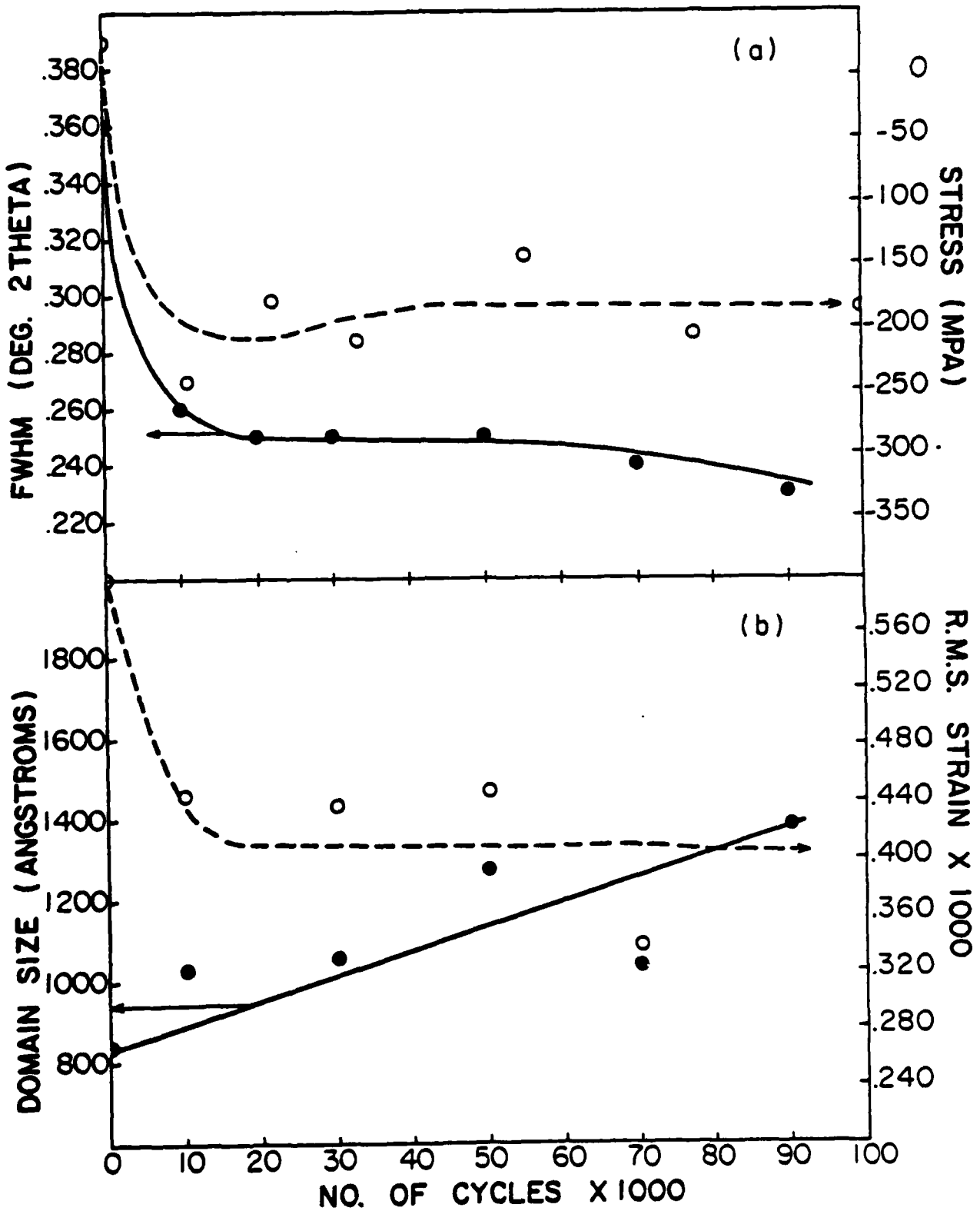
(a)
FWHM (DEG. 2THETA)
.380
.360
.340
.320
.300
.280
.260
.240
.220
STRESS (MPA)
0
-50
-100
-150
-200
-250
-300
-350
(b)
DOMAIN SIZE (ANGSTROMS)
1800
1600
1400
1200
1000
800
R.M.S. STRAIN X 1000
.560
.520
.480
.440
.400
.360
.320
.280
.240
0
10
20
30
40
50
60
70
80
90
100
NO. OF CYCLES X 1000

FIGURE 5

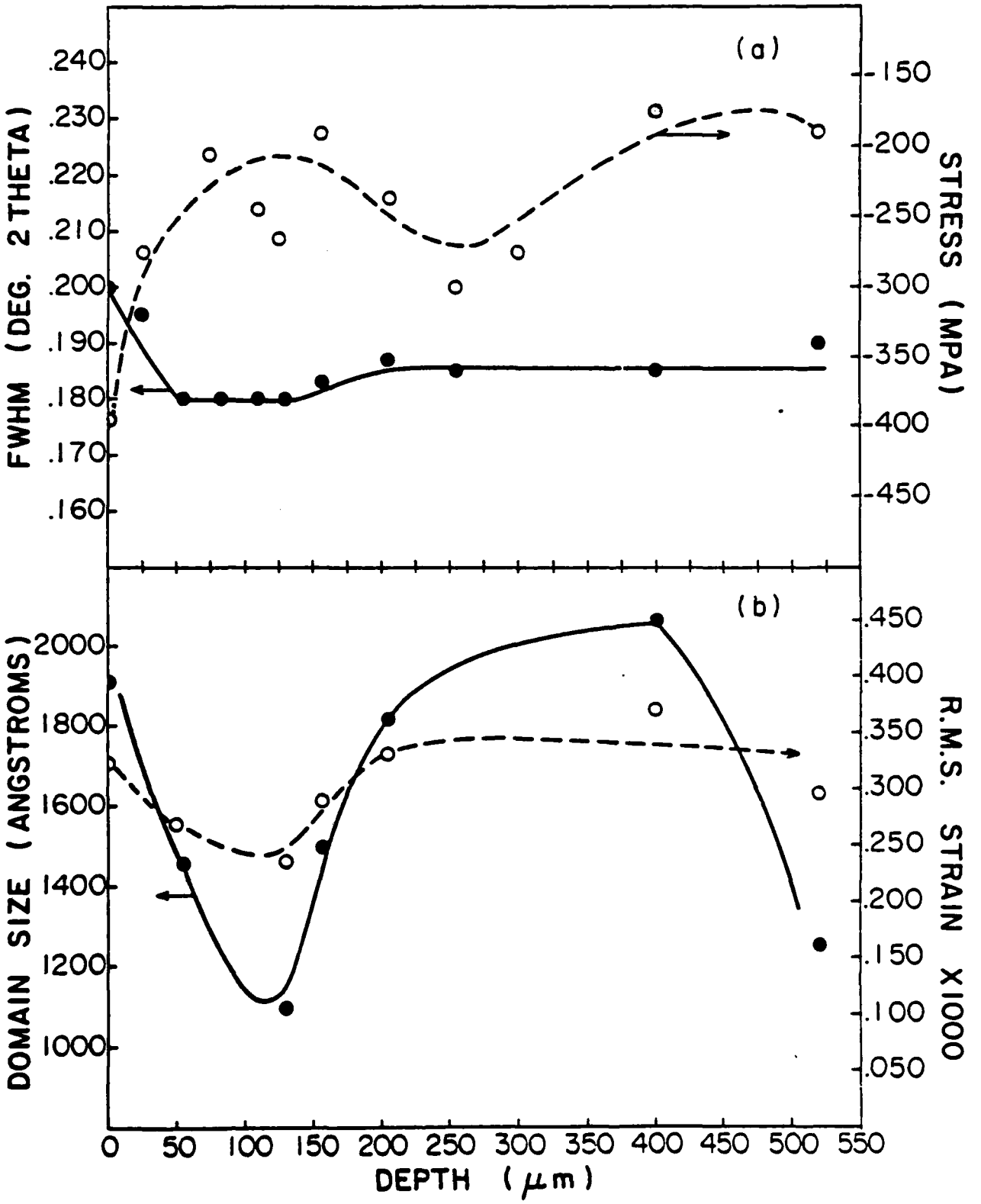

FIGURE 6

H. K. Kuo and J. B. Cohen

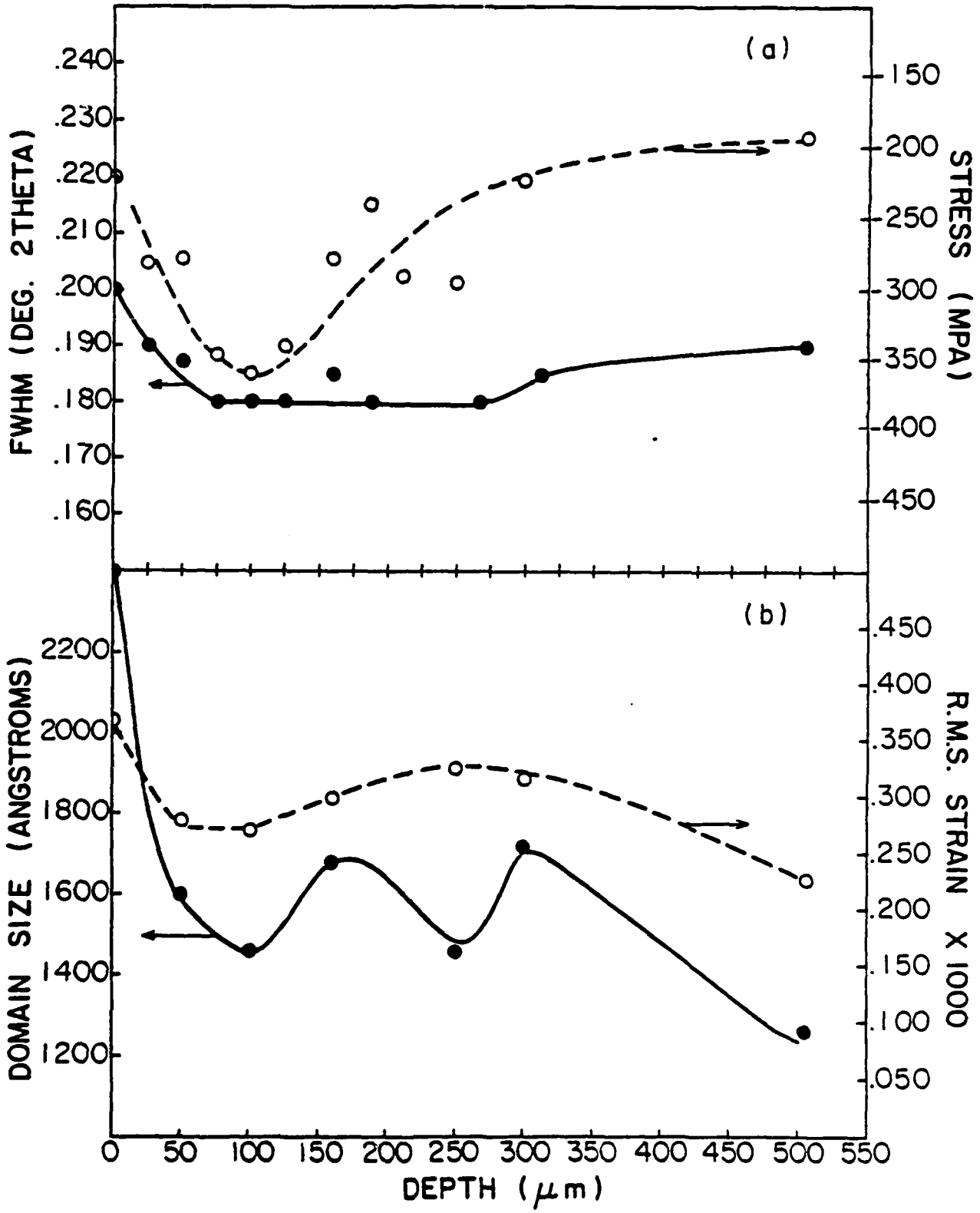

FIGURE 7

H. K. Kuo and J. B. Cohen

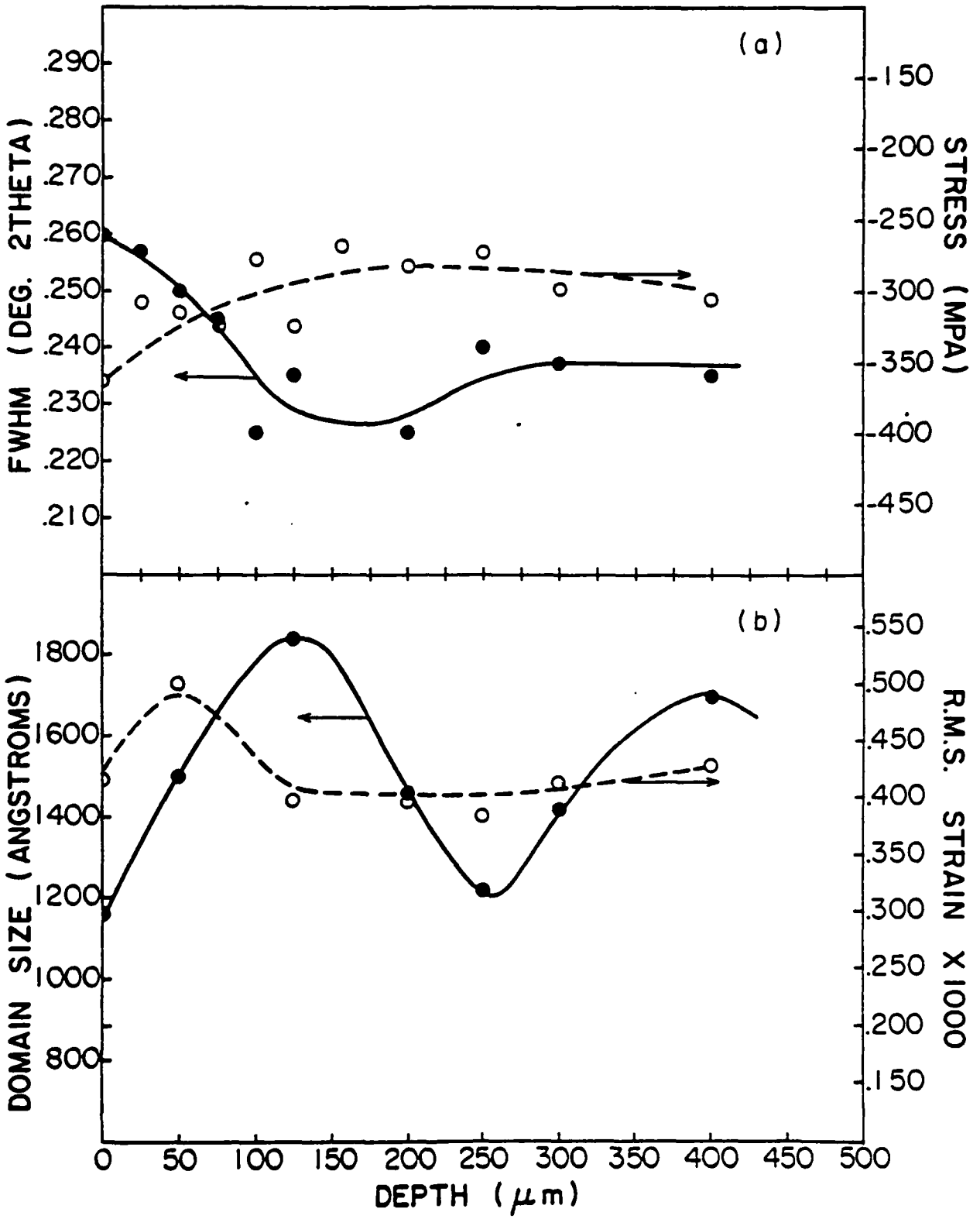

FIGURE 8

H. K. Kuo and J. B. Cohen

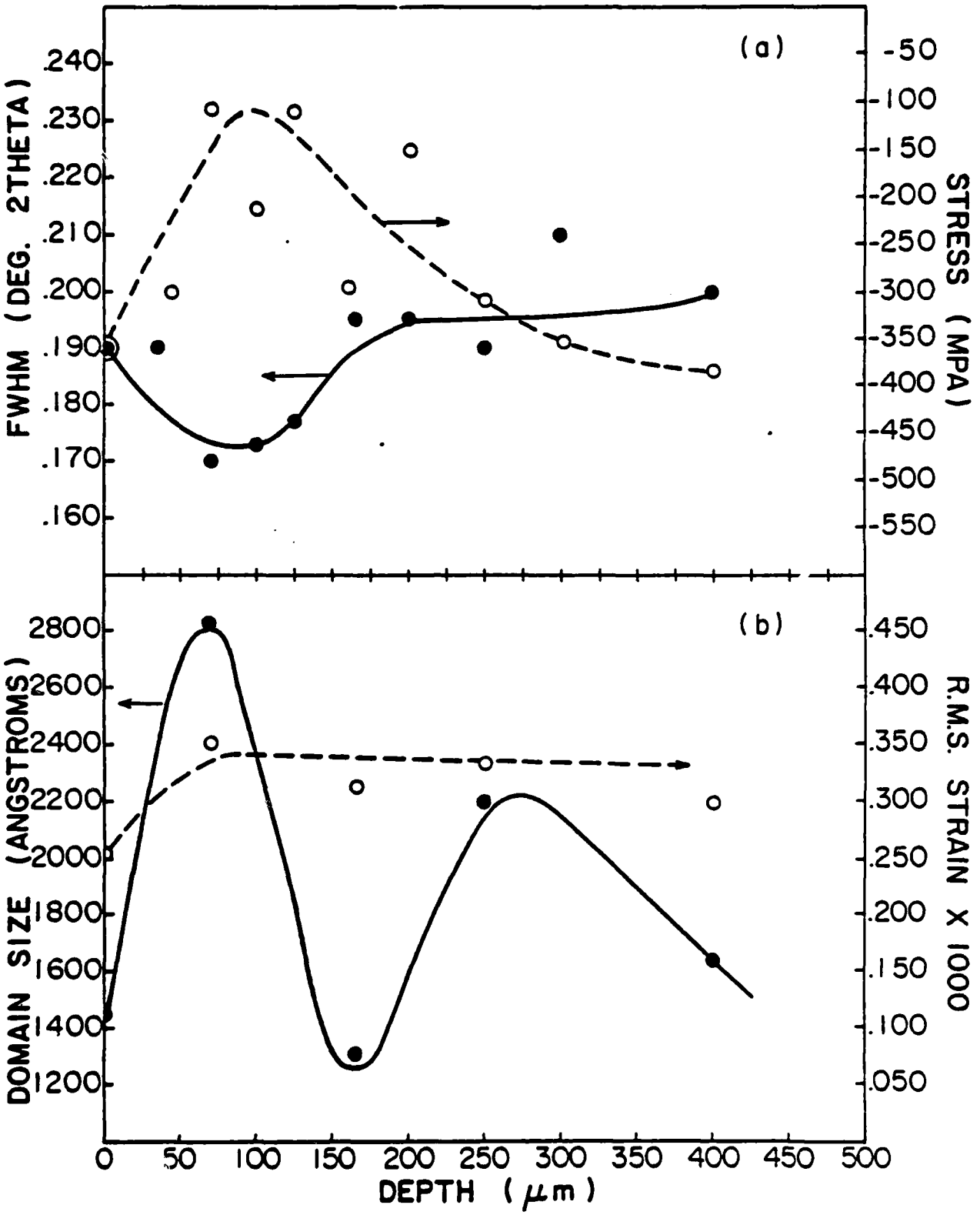
(a)
FWHM (DEG. 2THETA)
.240
.230
.220
.210
.200
.190
.180
.170
.160
STRESS (MPA)
-50
-100
-150
-200
-250
-300
-350
-400
-450
-500
-550
(b)
DOMAIN SIZE (ANGSTROMS)
2800
2600
2400
2200
2000
1800
1600
1400
1200
R.M.S. STRAIN X 1000
.450
.400
.350
.300
.250
.200
.150
.100
.050
0
50
100
150
200
250
300
350
400
450
500
DEPTH (μm)

FIGURE 9

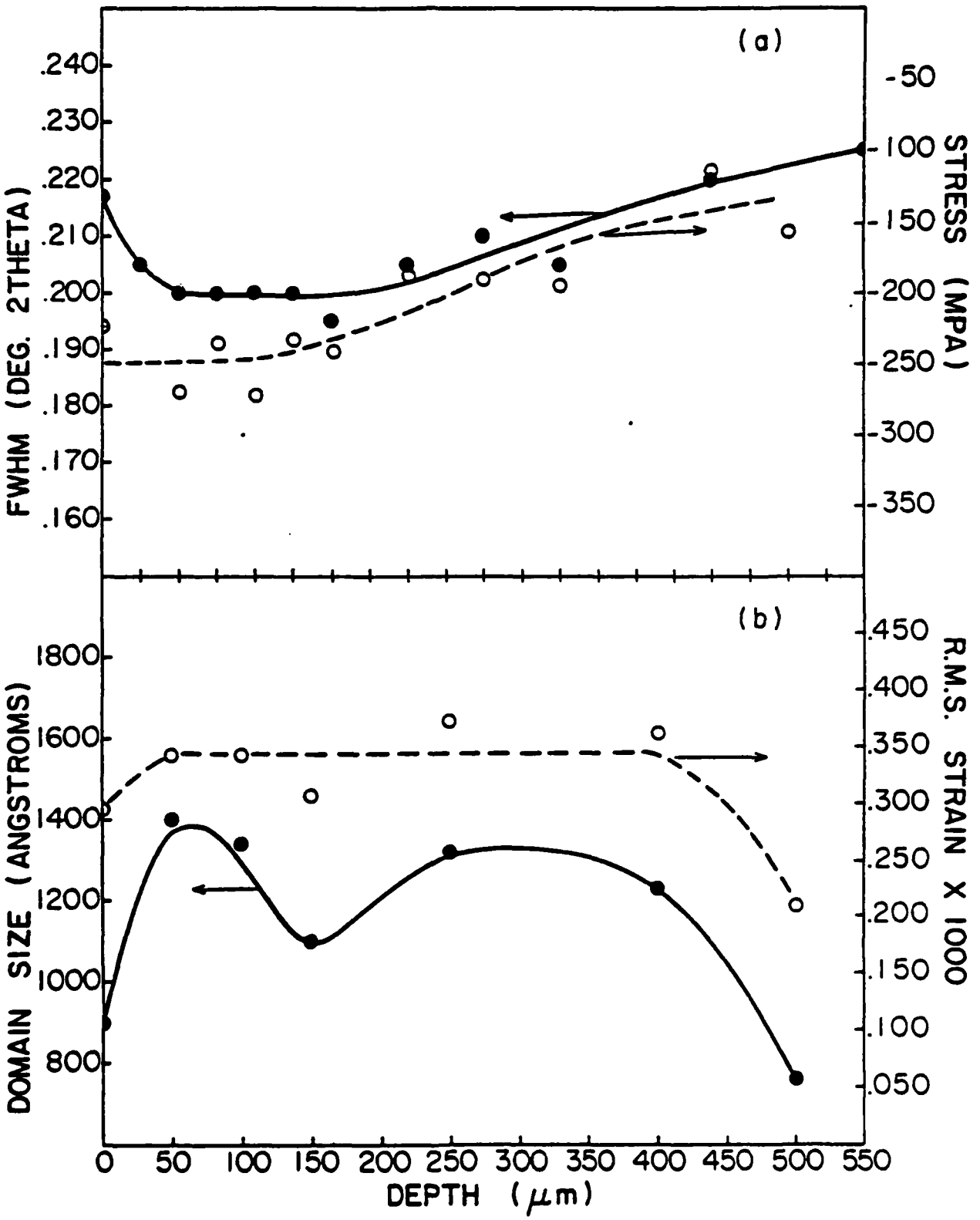
(a)
FWHM (DEG. 2THETA)
.240
.230
.220
.210
.200
.190
.180
.170
.160
STRESS (MPA)
-50
-100
-150
-200
-250
-300
-350
(b)
DOMAIN SIZE (ANGSTROMS)
1800
1600
1400
1200
1000
800
R.M.S. STRAIN X 1000
.450
.400
.350
.300
.250
.200
.150
.100
.050
0 50 100 150 200 250 300 350 400 450 500 550
DEPTH (μm)

FIGURE 10

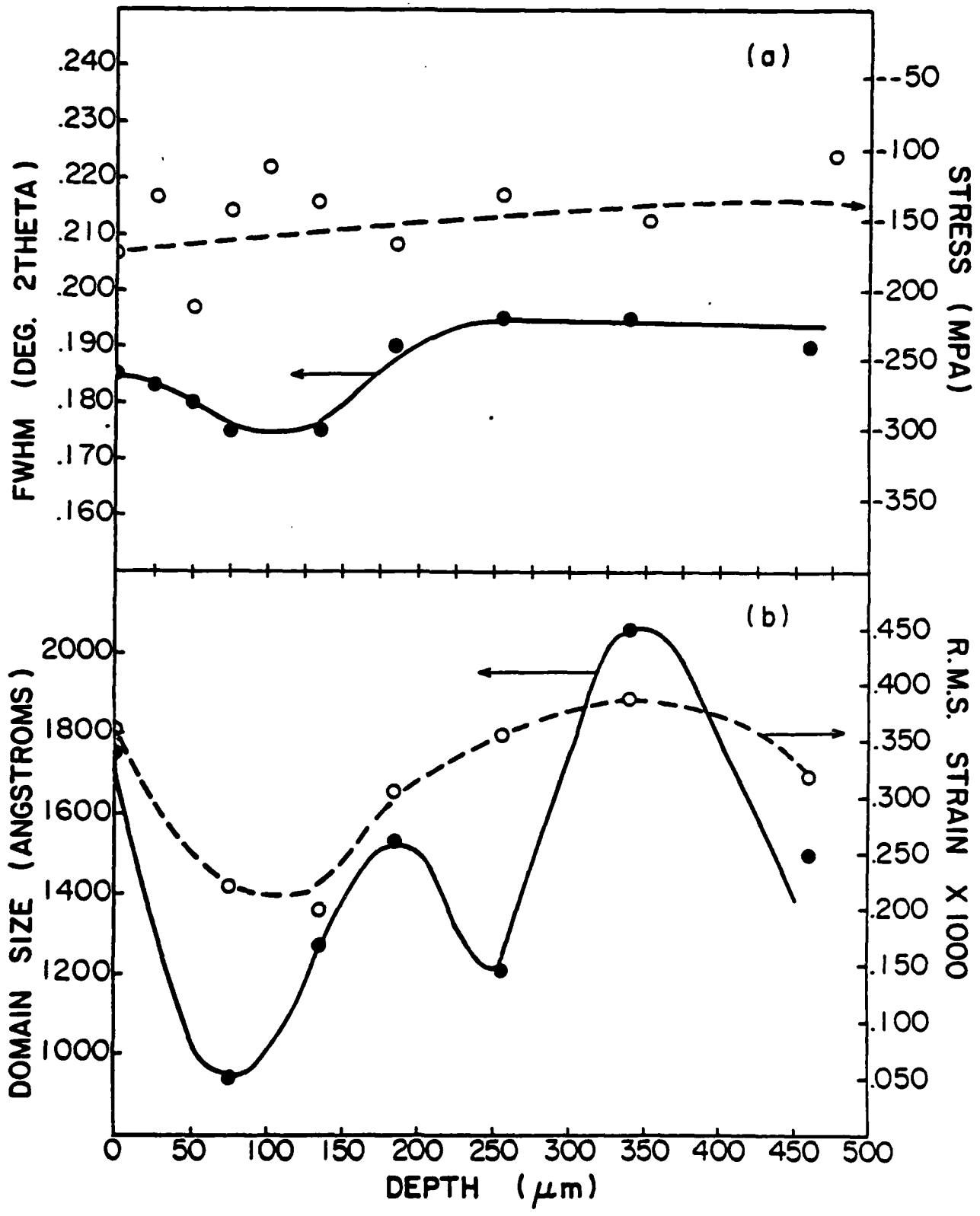
(a)
FWHM (DEG. 2THETA)
.240
.230
.220
.210
.200
.190
.180
.170
.160
STRESS (MPA)
-50
-100
-150
-200
-250
-300
-350
(b)
DOMAIN SIZE (ANGSTROMS)
2000
1800
1600
1400
1200
1000
R.M.S. STRAIN X 1000
.450
.400
.350
.300
.250
.200
.150
.100
.050
0
50
100
150
200
250
300
350
400
450
500
DEPTH (μm)

FIGURE 11

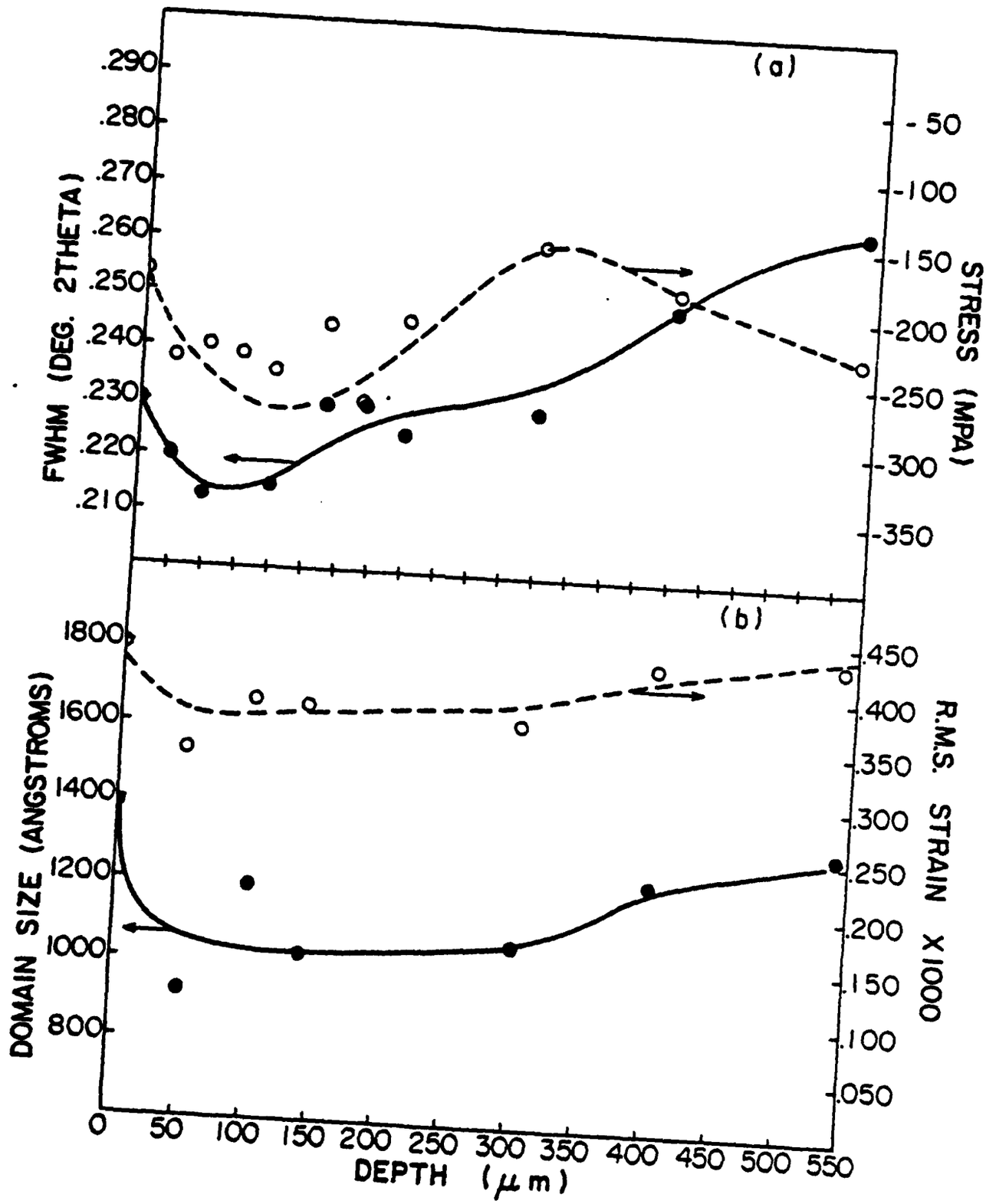

FIGURE 12

H. K. Kuo and J. B. Cohen

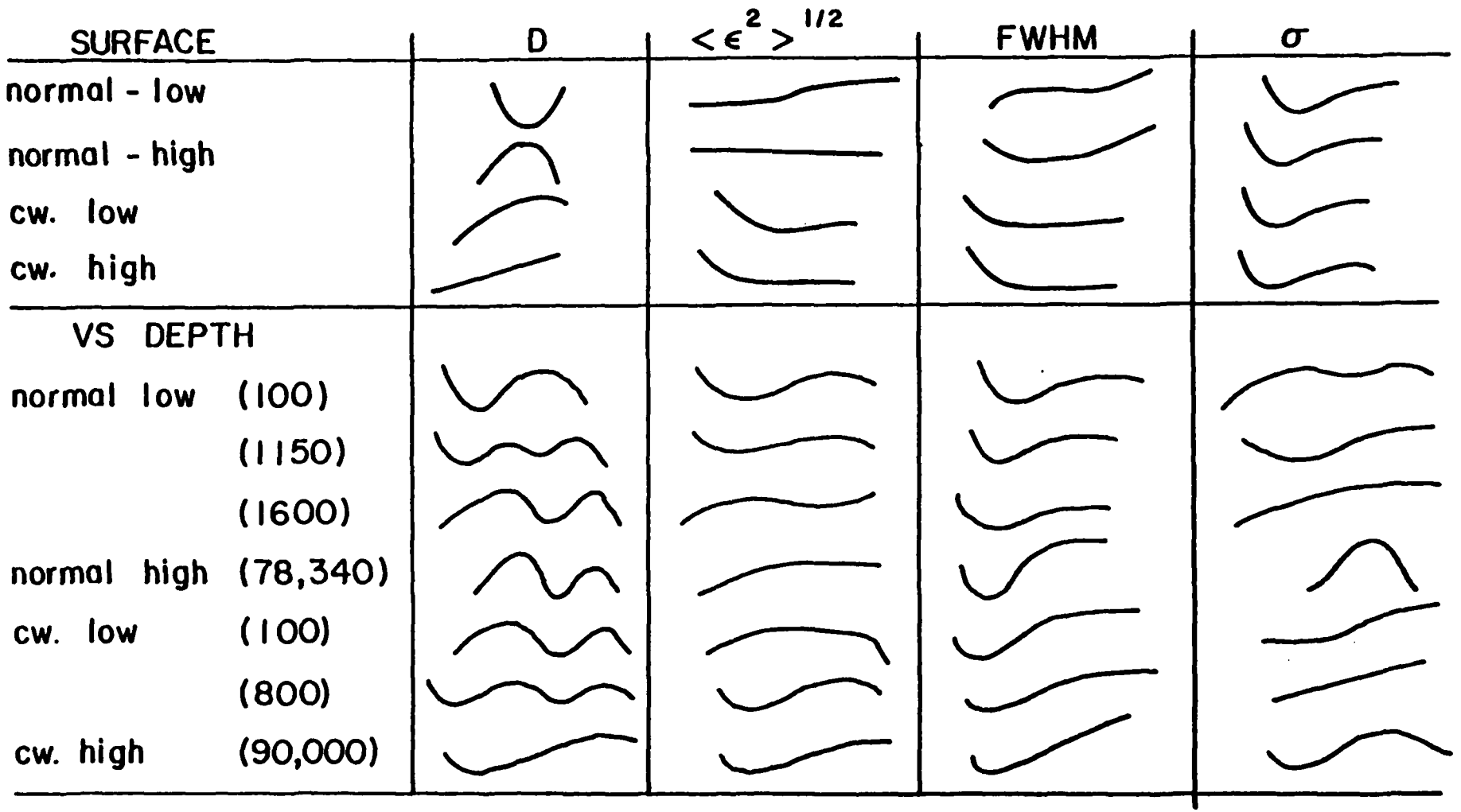
SURFACE
D
$<\epsilon^2>^{1/2}$
FWHM
σ
normal - low
normal - high
cw. low
cw. high
VS DEPTH
normal low (100)
(1150)
(1600)
normal high (78,340)
cw. low (100)
(800)
cw. high (90,000)

FIGURE 13

Security Classification

DOCUMENT CONTROL DATA - R & D

Security classification of title, body of abstract and indexing annotation must be entered when the overall report is classified)

1. ORIGINATING ACTIVITY (Corporate author) J. B. Cohen Northwestern University Evanston, Illinois 60201	2a. REPORT SECURITY CLASSIFICATION Unclassified 2b. GROUP

3. REPORT TITLE

CHANGES IN RESIDUAL STRESS, DOMAIN SIZE AND MICROSTRAIN DURING FATIGUE OF 1008 STEEL

4. DESCRIPTIVE NOTES (Type of report and inclusive dates)

Technical Report No. 9

5. AUTHOR(S) (First name, middle initial, last name)

H. K. Kuo and J. B. Cohen

6. REPORT DATE	7a. TOTAL NO. OF PAGES	7b. NO. OF REFS
March 1, 1983	34	25

8a. CONTRACT OR GRANT NO. N00014-80-C-0116 b. PROJECT NO. Mod. No. P00002 c. d.	9a. ORIGINATOR'S REPORT NUMBER(S) 9 9b. OTHER REPORT NO(S) (Any other numbers that may be assigned this report)

10. DISTRIBUTION STATEMENT

Distribution of this document is unlimited

DISTRIBUTION STATEMENT A
Approved for public release; Distribution Unlimited

11. SUPPLEMENTARY NOTES	12. SPONSORING MILITARY ACTIVITY
	Metallurgy Branch Office of Naval Research

13. ABSTRACT

Changes in the positions and shapes of x-ray diffraction peaks have been examined after low-cycle and high-cycle strain-controlled fatigue of normalized and cold-worked 1008 steel. Measurements were made at and below the surface. Domain (mosaic) size is sometimes the major contributor to peak breadth, but sometimes it is controlled by microstrain, or by both quantities. Microstrains are larger after low-cycle fatigue than after high-cycle fatigue. The surface residual stress is altered by fatigue, and the pattern of change with cycling is similar for low or high strains, and for initially normalized or cold-worked specimens. Near failure in low-cycle fatigue of a cold-worked specimen. Near failure in low-cycle fatigue of a cold-worked specimen, the domain size and microstrain approach those for a (cycled) annealed specimen. Dislocation densities are the order of 10^{13}-10^{14} per m^2. Cycling in the initially normalized condition increases both the dislocation density and dislocation arrangements with low long-range strain. However, with cold-worked 1008 steel, the density decreases and, near failure, the dislocation array is nearly random. In all cases, the peak breadth passes through a minimum vs. depth below the surface. In low-cycle fatigue of the normalized condition, the damage is less in the interior than at the surface, but after high-cycle fatigue, (and after high or low-cycle fatigue of cold-worked samples) the damage is greater in the interior of a specimen. The dislocation arrangement oscillates with depth, below the surface, at least for the first few hundred microns.

DD FORM 1 NOV 65 1473 (PAGE 1)

S/N 0101-807-6801

Security Classification

14. KEY WORDS	LINK A		LINK B		LINK C	
	ROLE	WT	ROLE	WT	ROLE	WT
residual stresses, line broadening, fatigue of steel, low-cycle fatigue, high-cycle fatigue.						


4-8
DTI